

# Shear Localization in Mantle Peridotites Accompanied with Successive Transformation of Deformation Condition, Microstructure and Rheology

Takashi SAWAGUCHI\*

## Abstract

This paper is aimed at describing hierarchical shear localization (km-, tens of meter- and cm-scale) in the Horoman peridotite complex, Hidaka metamorphic belt, northern Japan. Shear localization continued throughout retrograde conditions of metamorphism, successively from granulite ( $\geq 900^{\circ}\text{C}$ ) to amphibolite (ca.  $700^{\circ}\text{C}$ ) facies, evidence for which is preserved in spatial variation of syn-kinematic amphibole reaction rims around Opx porphyroclasts. Deformation mechanisms and rheology in the shear zones suggest that shear localization in the Horoman peridotites resulted in weakening of strength by an order of 3~4 due to grain-size reduction.

**Keywords** : shear localization, Horoman peridotites, rheology

## 1. INTRODUCTION

Rocks may undergo shear localization, forming faults and shear zones, in both brittle and ductile regimes, depending on the deformation conditions and the mechanical properties of the rocks (Poirier, 1980, White et al., 1980, Drury et al., 1991). Shear localization in rocks under high temperature and pressure conditions leads to development of a high strain zone, which can be recognized by intense foliation development and grain-size reduction. Such zones on micro- to macroscopic scales are observed in naturally deformed crustal and mantle rocks, and also detected by deep seismic reflection profiling (BIRPS; Brewer et al., 1983) as gently dipping thrusts in the mid to lower crust which transects the Moho discontinuity into the upper mantle. On the other hand, extensional mantle shear zones are presumed to develop in rifting environments (Rutter and Brodie, 1988, Vissers et al., 1995). The movement along these mantle shear zones is responsible for the uplift and emplacement of upper mantle peridotite massifs (Boillot et al., 1987, Rutter and Brodie, 1988, van der Wal and Vissers, 1993, Vissers et al., 1995).

---

\*) Natural Science Laboratory, Toyo University, 5-28-20 Hakusan, Bunkyo-ku, Tokyo 112-8606, Japan

Tectonic emplacement of peridotite massifs along these shear zones must cause changes in deformation conditions such as temperature, pressure and strain rate. Metamorphic reactions accompanying with these changes generally facilitate plastic deformation ("reaction weakening", White and Knipe, 1978, Rubie, 1983, 1990, Rutter and Brodie, 1995). An emplacement process and history of Alpine-type peridotite massifs in orogenic belts can be reconstructed from microstructural evidence of transformation of deformation conditions by metamorphic reactions in a shear zone.

The Horoman peridotite complex provides a good opportunity to investigate the relationship between deformation and metamorphism in a mantle shear zone (Sawaguchi, 2004). The purpose of this paper is to describe hierarchical shear localization (km-, tens of meter- and cm-scale) in the Internal Shear Zone, and to demonstrate that shear localization continued throughout retrograde conditions of metamorphism, successively from granulite ( $\geq 900^{\circ}\text{C}$ ) to amphibolite (ca.  $700^{\circ}\text{C}$ ) facies, evidence for which is preserved in spatial variation of syn-kinematic amphibole reaction rims around Opx porphyroclasts. Deformation mechanisms and rheology in the shear zones will be discussed by reference to deformation mechanism maps for wet olivine polycrystals, which suggest that shear localization in the Horoman peridotites resulted in weakening of strength by an order of 3~4 due to grain-size reduction.

## 2. HIERARCHICAL SHEAR LOCALIZATION IN THE SHEAR ZONE

Grain-size reduction of polygonal olivine matrix in the "Laminated-mosaic-porphyroclastic texture" (Harte, 1977) are recognized in from the Equigranular Zone to the Internal Shear Zone. Except rarely very fine-grained sample at the northern end of the complex, samples at all section in the Internal Shear Zone has about 200  $\mu\text{m}$  grain size of polygonal olivine. Several cm-scale shear zones were discovered in the Internal Shear Zone at the southwestern part of the complex (Figs. 1, 2; Otsukifushi-zawa River and the Konbu-no-sawa River section). Microstructure in the vicinity of the cm-scale shear zone has about 200  $\mu\text{m}$  grain size of polygonal olivine but recrystallized orthopyroxene + olivine  $\pm$  clinopyroxene aggregates extend from the orthopyroxene porphyroclast forming continuous anastomosing matrix. These textural variations suggest that the Internal Shear Zone has a character of hypothetical shear localization. In this paper, microstructures in the Equigranular Zone and the Internal Shear Zone are subdivided into 4 classes (class 0~3, Fig. 3), and shear localization between each class is described below. Microstructure in the Equigranular Zone is referred as class 0. In the Internal Shear Zone, microstructure without forming continuous anastomosing matrix of recrystallized orthopyroxene + olivine  $\pm$  clinopyroxene aggregates is referred as class 1 and that with forming continuous anastomosing matrix is referred as class 2, respectively.

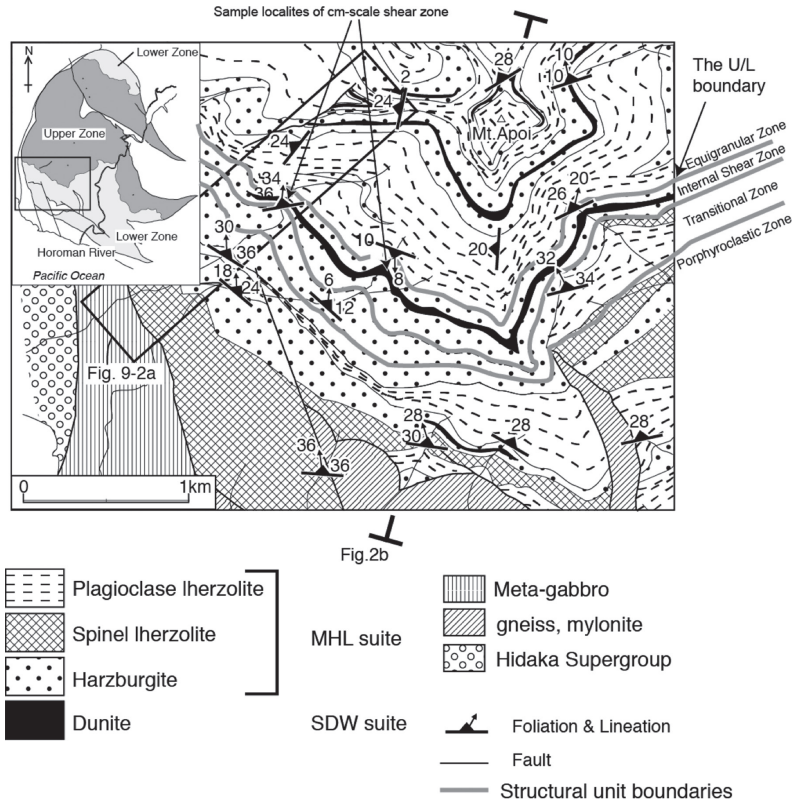


**Fig. 1** Geological map of the south-western part of the Horoman peridotite complex. The foliations are parallel to the compositional layering, dipping gently to moderately northward. The U/L zone boundary indicates the Upper/Lower zone boundary. MHL and SDW suites are defined by Takahashi (1991). The MHL (Main Harzburgite–Lherzolite) suite is a residual mantle peridotite. The SDW (Spinel-rich Dunite–Wehrlite) suite is a cumulate from a magma segregated from the surrounding MHL suite.

Microstructure in the cm-scale shear zone is referred as class 3. Harzburgite was selected for sample analysis because typical shear localized microstructures are observed in olivine-rich peridotites. Over three hundred oriented samples were collected from the whole massif and two typical samples from each of the four classes were chosen for this study.

### 2.1 Class 0 to 1 (kilometer-scale) shear localization

Class 0 deformation microstructure shows a typical equigranular texture and is distributed in the uppermost part of the massif (Fig. 3a). The average grain-size of polygonal olivine decreases gradually with depth and the microstructure changes into class 1 on a km-scale (Figs. 2, 3b). Class 1 still preserves the uniform grain size of olivine with polygonal form, and scarce substructures such as subgrain walls and kink bands are

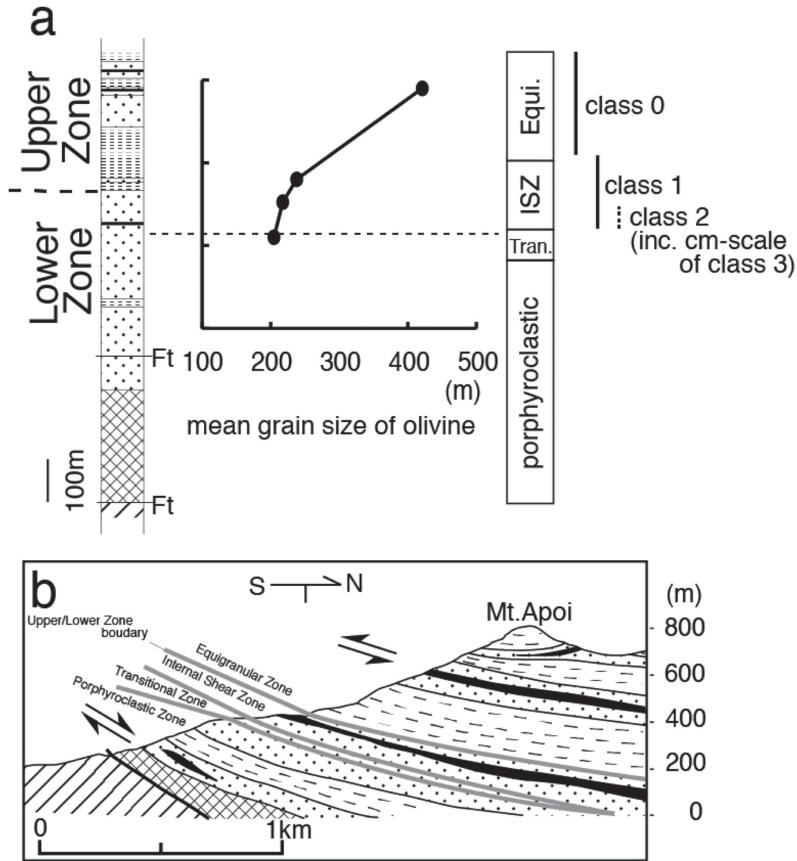


**Fig. 2** (a) Columnar section with which the distribution of the different deformation microstructures are shown. The mean grain size of polygonal olivine grains in the Equigranular Zone and the Internal Shear Zone is also shown. (b) Cross-section showing senses of shear

found, or these are widely spaced if any. Orthopyroxene in class 1 have a large grain size relative to olivine, and amount to ca. 5% (Fig. 4). Fine-grained Opx + Ol  $\pm$  Cpx aggregates occur at the rims of large Opx grains extending toward the foliation, but do not connect to form continuous fine-grained bands (Fig. 5a). The grain size of olivine in this aggregate is ca. 50  $\mu$ m. Strong concentration of lattice preferred orientation (LPO) of polygonal olivine implies that both class 0 and class 1 deformation microstructures are associated with dislocation creep process (Fig. 6).

## 2.2 Class 1 to 2 (several tens of meter-scale) shear localization

Class 2 deformation microstructure is characterized by continuous anastomosing matrix composed mainly of Opx + Ol  $\pm$  Cpx aggregates extending from large Opx grains (Fig. 3c). The transition from class 1 to 2 is assumed to be in the range of meters to several tens of meters judging from class 2 distribution in several outcrops. Class 2 is re-

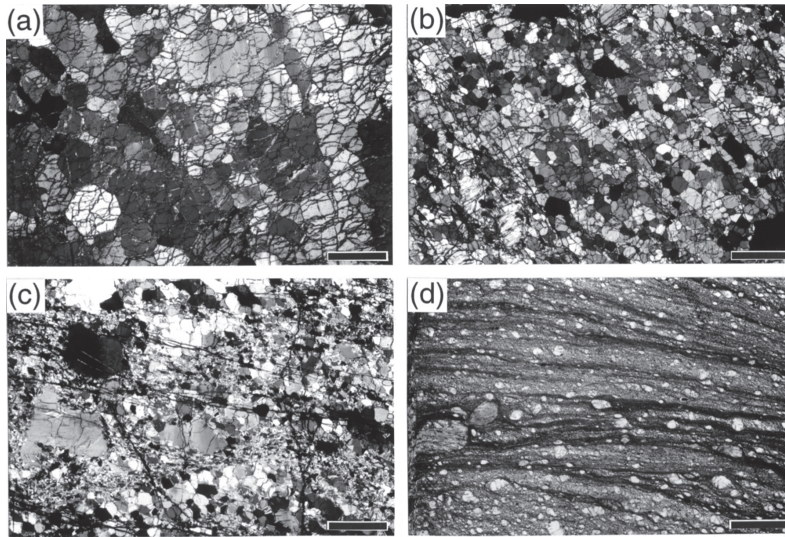


**Fig. 3** Photomicrographs of the typical deformation microstructures in the Horoman peridotites. (a) class 0 (b) class 1 (c) class 2 (d) class 3. scale bar is 1 mm. (XPL)

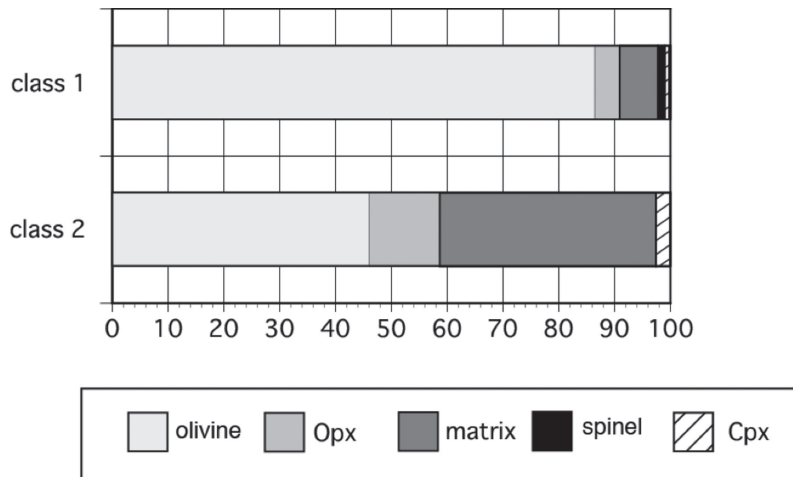


**Fig. 4** Modal compositions of class 1 and 2 peridotites.

stricted to the lower part of the class 1 distributed region (Fig. 2). Large Opx porphyroclasts have reaction rims of pargasitic hornblende parallel to the foliation (Fig. 5b). A few small grains of pargasitic hornblendes can be also observed in the fine-grained Opx + Ol  $\pm$  Cpx matrix. The average grain size of the matrix is ca. 50  $\mu$ m. The modal composition of Opx porphyroclast increases from 5 % in class 1 to 13% in class 2 accompanying by increase in the matrix from 7 % in class 1 to 39% in class 2 (Fig. 4).

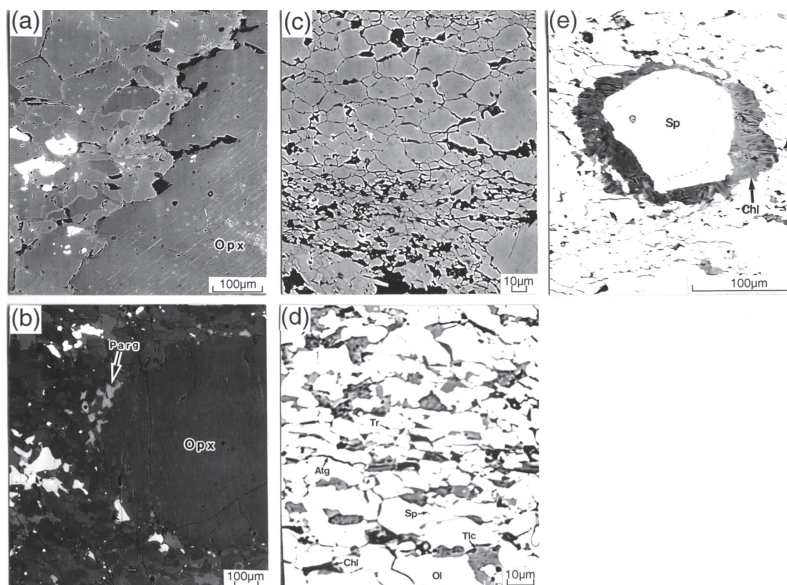


**Fig. 5** BSE images of deformation microstructures. (a) Recrystallized Opx + Ol aggregate at the rim of large Opx grains extending toward the foliation in class 1 peridotite (b) Reaction rim of pargasitic hornblende recrystallized in the vicinity of large Opx grains parallel to the foliation in class 2 peridotite. (c) Fine-grained (upper) and ultra-fine-grained (lower) matrix in class 3 peridotite. (d) Chlorite fibers growing from the fine-grained magnesiochromite aggregates with relic Cr-spinel cores parallel to the foliation.

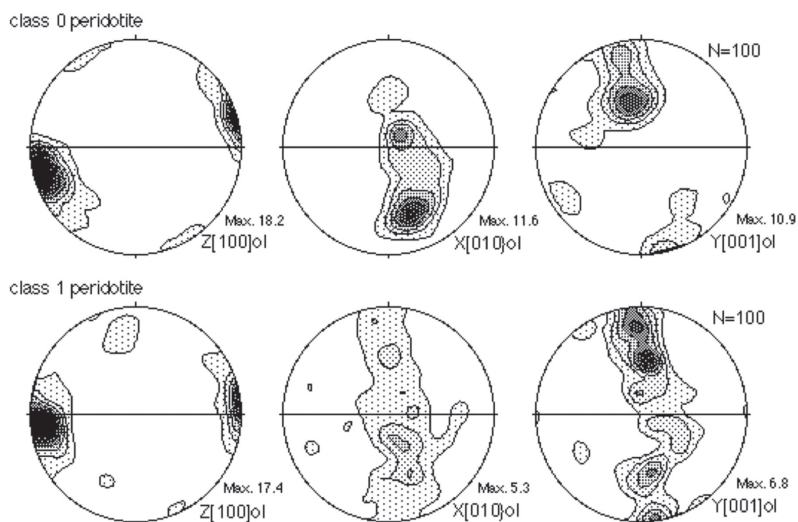


**Fig. 6** Lattice preferred orientation of olivine in class 0 and 1 peridotites. Horizontal line represents the foliations whereas points of both ends on the foliation represent the lineation. Max. means maximum density. Lower hemisphere, equal-area projection. 100 grains were measured.

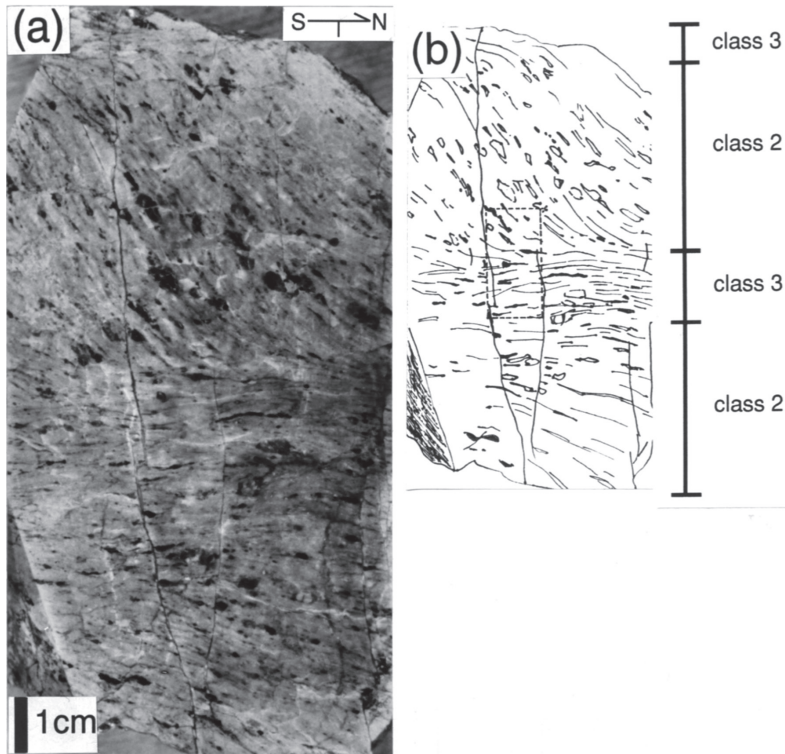


**Fig. 7** (a) Polished surface of the class 2-3 shear zone (Foliation normal and lineation parallel) (b) Sketch drawing. Dashed rectangle outlines the photomicrograph of Fig. 8

### 2.3 Class 2 to 3 (cm-scale) shear localization

Several cm-scale shear zones (class 3) can be observed in class 2 peridotites. Class 3 shear zones transected either oblique or parallel to the foliation in class 2. Figure 7 and 8 show progressive bending of the foliation within class 2 into the plane of the mylonitic foliation within class 3 shear zone. The class 2 peridotite lying between class 3 shear zone (Figs. 7, 8) preserves almost equant olivine, but very fine olivine grains occur along grain boundaries.

In the class 3 peridotites, the polymineralic fine-grained (10~100  $\mu\text{m}$ ) matrix and olivine and Opx porphyroclasts (ca. 200  $\mu\text{m}$ ) are separated by thin (100~250  $\mu\text{m}$ ), anastomosing ultra-fine-grained (2~30  $\mu\text{m}$ ; ca. 10  $\mu\text{m}$ ) bands (Figs. 3d, 5c). Both fine-grained matrix and ultra-fine-grained bands are composed of  $\text{Ol} + \text{Tr} + \text{Chl} + \text{Tlc} + \text{Atg} + \text{Spl}$  ( $\pm$  Opx). Modal percent of the hydrous minerals in ultra-fine-grained bands is larger than that in fine-grained layer (Fig. 9). Talc grains are recrystallized in close association with antigorite and olivine in ultra-fine-grained bands (Fig. 5d). Ultra fine-grained bands are thought to be inherited from the fine-grained  $\text{Opx} + \text{Ol} \pm \text{Cpx}$  aggregates in class 2,

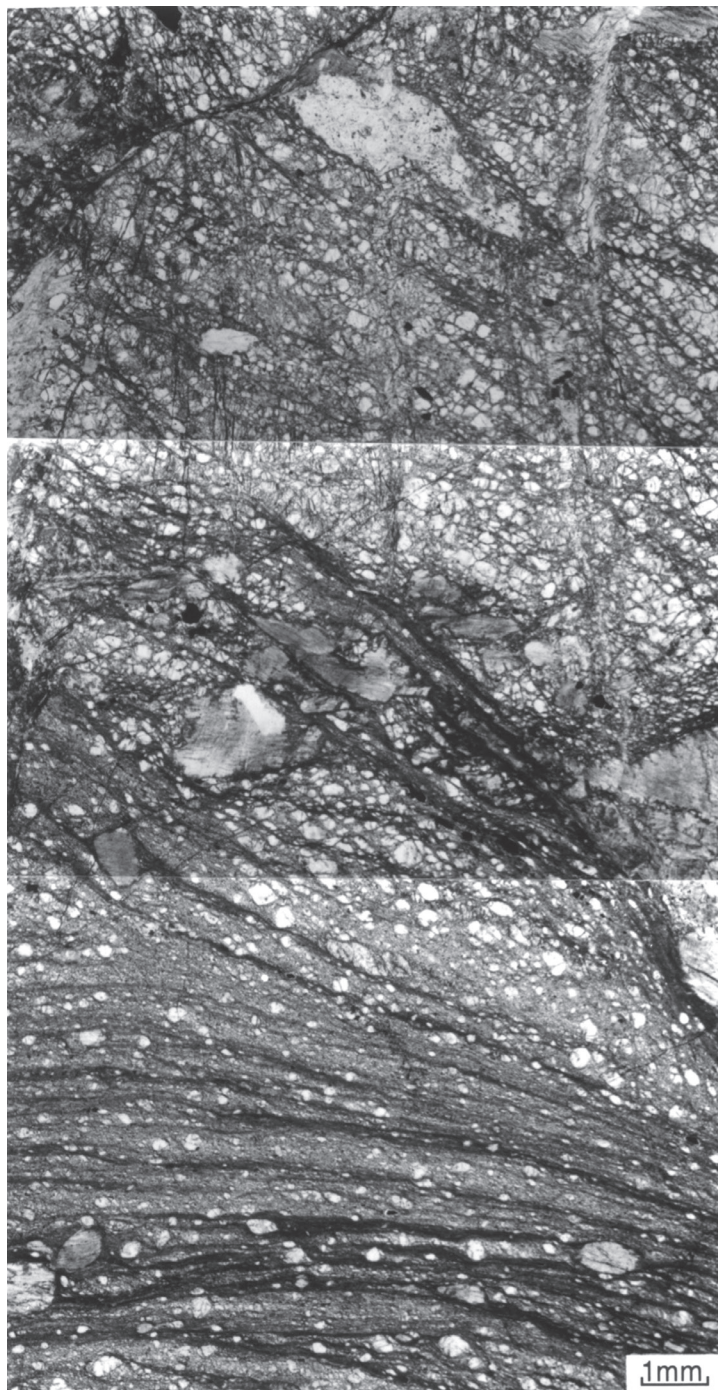


**Fig. 8** Photomicrograph of the class 2-3 shear zone. The area is shown in Fig. 7(b). The fluidal microstructure in class 3 peridotite is defined by dark colored ultra fine-grained band and the lighter colored fine-grained matrix. (PPL).

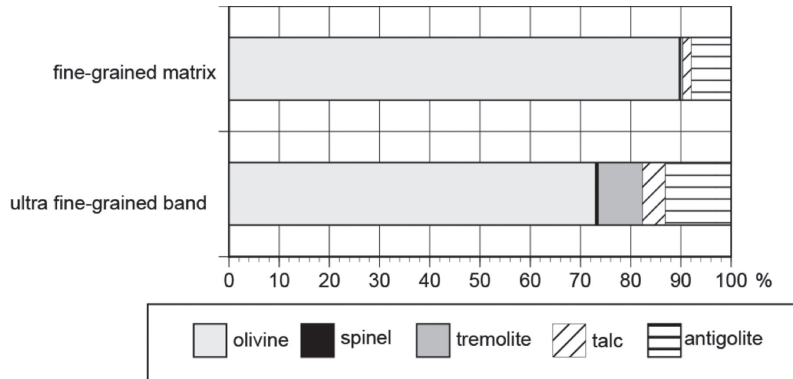


**Fig. 9** Modal compositions of fine-grained and ultra-fine-grained matrix in class 3 peridotite, determined by image analysis for BSE image with NIH-Image software.

because the bands extend from the large Opx porphyroclasts or their pseudomorphs. Olivine-rich, fine-grained matrix is also thought to be inherited from dynamically recrystallized olivine grains.

Although various hydrous minerals such as tremolite, chlorite, talc and antigorite in ultra fine-grained bands indicate that the development of class 2-3 shear localization was associated with fluid infiltration and hydration of the peridotite, it is difficult to distinguish syn-kinematic products from later alteration judging only from the mineral assemblage in ultra fine-grained bands and matrix. The compositions of tremolite, chlorite and talc in both fine-grained matrix and ultra-fine-grained band are shown in Fig. 10 and Table 1.

### 3. SYN-TECTONIC REACTION RIM OF HYDROUS MINERALS AROUND ORTHOPYROXENE PORPHYROCLASTS

Large Opx porphyroclasts have reaction rims of pargasitic hornblende parallel to the foliation in Class 2 peridotite. In Class 3 peridotite, asymmetric reaction rims of fibrous tremolite and olivine form around the Opx porphyroclasts or pseudomorph (Fig. 11). The tremolite rims are 10~30  $\mu\text{m}$  in width and grew from the margin of the Opx porphyroclast pseudomorph which is replaced by talc + antigorite. Pargasitic hornblendes which have sharp contacts with tremolite are included in fibrous tremolite grains (170~400  $\mu\text{m}$  away from the orthopyroxene pseudomorph along the tremolite zone). The pargasitic hornblende grains have sharp, straight contacts with tremolite. Anthophyllite occurs as rims of the Opx pseudomorphs. The composition of pargasitic hornblende, tremolite and anthophyllite in reaction rim is shown in Fig. 10 and Table 1. Talc does not form as a reaction rim with these amphiboles, but replaces the orthopyroxene por-

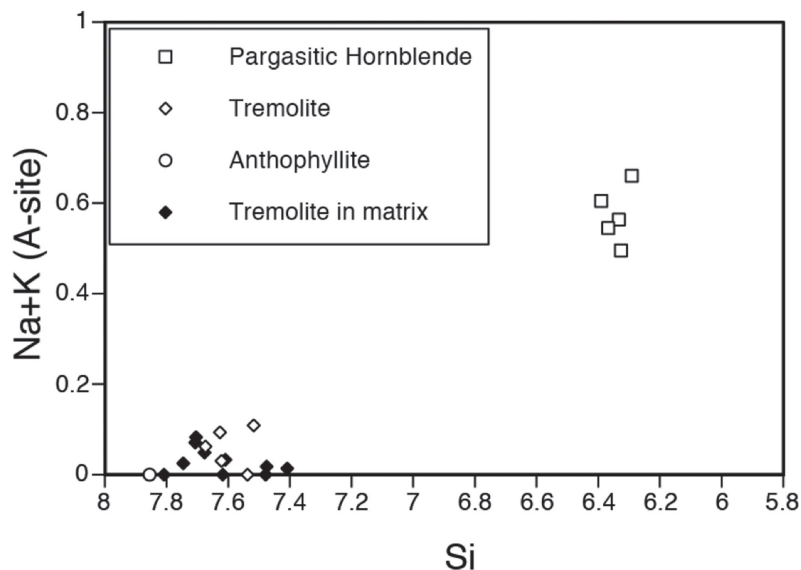


**Fig. 10** The chemical composition of amphiboles in Opx reaction rim and tremolite in mylonite matrix plotted within (Na + K) in A site - Si diagram.

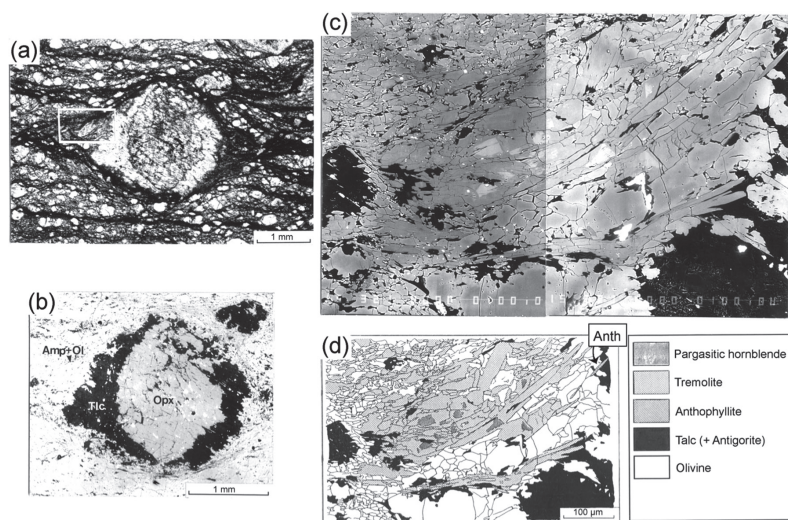


**Fig. 11** Opx porphyroclast and syn-kinematic reaction rims of amphiboles + olivine in class 3 peridotite (Sawaguchi, 2004). (a) Photomicrograph. PPL (b) BSE image (c) BSE image of syn-kinematic amphiboles + olivine reaction rims (d) Schematic illustration showing the distribution of pargasitic hornblende, tremolite and anthophyllite. Note that pargasitic hornblendes have a sharp contact with tremolite in the core and the anthophyllite grain has grown on the rim of the Opx porphyroclast pseudomorph. Opx pseudomorph is composed of talc + antigorite.

**Table 1** Average chemical composition of hydrous minerals in reaction rims and mylonite matrix. Alkali cations (Na + K) in A-site for amphiboles are calculated from Rock and Leake (1984).

Minerals	reaction rim around Opx			Sp rim	mylonite matrix		
	Pargasitic Hb.	Tremolite	Anthophyllite	Chlorite	Tremolite	Chlorite	Talc
Analysis no.	5/average	5/average	1grain	2/average	10/average	3/average	3/average
SiO <sub>2</sub>	45.05	54.49	56.30	34.21	55.97	30.95	61.54
TiO <sub>2</sub>	0.25	0.02	0.00	0.00	0.04	0.04	0.12
Al <sub>2</sub> O <sub>3</sub>	13.71	3.25	1.71	15.02	3.30	19.33	0.65
Cr <sub>2</sub> O <sub>3</sub>	2.91	0.95	0.04	0.47	0.29	0.07	0.00
FeO	3.16	2.46	6.23	2.58	2.44	2.83	1.34
MnO	0.14	0.06	0.51	0.00	0.14	0.04	0.00
MgO	17.75	22.10	28.75	32.82	23.07	31.38	29.67
CaO	12.80	12.61	0.60	0.03	12.85	0.07	0.03
Na <sub>2</sub> O	1.97	0.52	0.12	0.07	0.36	0.03	0.27
K <sub>2</sub> O	0.59	0.04	0.00	0.19	0.02	0.02	0.09
Total wt%	98.32	96.52	94.25	85.39	98.49	84.76	93.70
Formula							
O	23	23	23	28	23	28	22
Si	6.342	7.596	7.852	6.523	7.623	5.955	7.959
Ti	0.026	0.002	0.000	0.000	0.004	0.006	0.012
Al	2.275	0.534	0.281	3.377	0.529	4.386	0.100
Cr	0.323	0.105	0.004	0.070	0.031	0.010	0.000
Fe	0.373	0.286	0.727	0.412	0.278	0.456	0.145
Mn	0.016	0.008	0.060	0.000	0.017	0.007	0.000
Mg	3.726	4.594	5.977	9.329	4.685	9.000	5.720
Ca	1.931	1.884	0.089	0.007	1.876	0.013	0.005
Na	0.537	0.142	0.033	0.024	0.095	0.012	0.068
K	0.106	0.007	0.000	0.047	0.004	0.004	0.014
Total	15.655	15.157	15.022	19.789	15.142	19.850	14.021
Mg/(Mg+Fe)	0.909	0.941	0.892	0.958	0.944	0.952	0.975
(Na+K) A site	0.574	0.059	0.000		0.024		

phyroclasts with antigorite from the rim toward the core. Thin films (1~3  $\mu\text{m}$  width) of antigorite also fill grain boundaries in the reaction rims.

Chlorite fibers grew from the fine-grained magnesiochromite aggregates with relic Cr-spinel cores parallel to the foliation (Fig. 5e). These chlorite reaction rims with a strong preferred orientation indicate syn-kinematic breakdown of spinel. The chemical composition of chlorite is shown in Table 1.

## 4. DISCUSSION

### 4.1 Shear localization during retrograde metamorphism

In previous studies of peridotite mylonites, inferred deformation conditions are mainly based on geothermometry of retrograde mineral assemblages, such as two-pyroxene pair or Mg-Fe exchange equilibrium between spinel and olivine (Jaroslow et al., 1996). These temperatures only represent snapshots of specific conditions of the temperature-time path. Evidence of evolutionary deformation conditions in peridotite mylonite is preserved in deformation microstructures, which are related to metamorphic reactions, such as reaction rims, porphyroblast growth patterns or microboudinage (Passchier and Trouw, 1996).

Shear localization in the Horoman peridotite complex, except for class 0-1, are associated with hydration reactions. Deformation conditions and their change during shear localization can be inferred from the synkinematic hydrous reaction rims in each class of deformation microstructure.

It is clear that class 1-2 shear localization was already initiated during granulite facies conditions accompanied with ingress of water, because pargasitic hornblende reaction rims are synkinematically recrystallized by the breakdown of Opx porphyroclasts parallel to the foliation in class 2 peridotites (Fig. 5b).

In the class 3 peridotites, tremolite grains with pargasitic hornblende cores grew from Opx pseudomorphs parallel to the foliation, and anthophyllite grains grew on the rims of the Opx pseudomorphs. The chemical composition of calcic amphiboles in ultramafic rocks correlates with metamorphic grade and the Si-content of the formula unit is the most sensitive compositional parameter reflecting metamorphic grade (Jenkins, 1981, 1983, Evans, 1982). Both the Upper and Lower Zones of the Horoman peridotite complex experienced rapid cooling near the boundary of the spinel-plagioclase peridotite stability field (Fig. 12; Ozawa and Takahashi, 1995). Taking this thermal history into account, the retrogressive change in deformation condition during shear localization is thought to be responsible for the spatial variation of amphibole reaction rims around Opx porphyroclasts. Rapid decrease in temperature during shear localization caused the change in chemical composition of amphibole reaction rims from pargasitic hornblende ( $\geq 900^{\circ}\text{C}$ ) through tremolite until anthophyllite (ca.  $700^{\circ}\text{C}$ ) (Fig. 12). The compositional gap between pargasitic hornblende and tremolite is considered to reflect that the composition of calcic amphiboles remains close to that of the tremolite end member until conditions high in the amphibolite facies are reached (Evans, 1982). Synkinematic chlorite fibers grew from spinel grains in the chlorite stability field ( $< 780^{\circ}\text{C}$ ).

The plastic deformation process in class 2-3 shear localization ceased during the talc stable condition, because talc does not form as a reaction rim with amphiboles, but re-

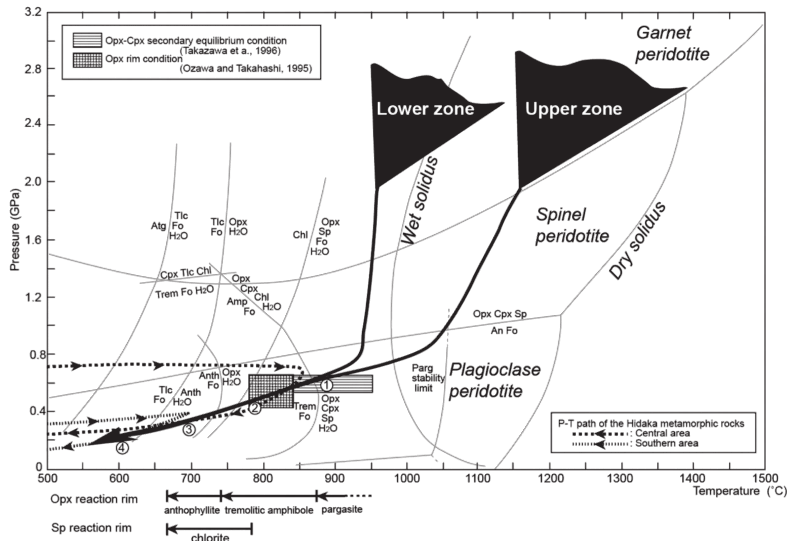


**Fig. 12** Inferred P-T trajectory of the peridotite mylonite in the Horoman peridotite complex (black), and that of the upper and lower zones (gray) after Ozawa and Takahashi (1995). Rectangle with stripe shows the secondary equilibrium temperatures inferred from the compositions of Opx exsolution lamellae and its host clinopyroxene and compositions of Cpx coexisting with Opx in the fine-grained seams (Takazawa et al. 1996). Rectangle with cross pattern shows the minimum P-T conditions inferred from the rim compositions of pyroxenes (Ozawa and Takahashi, 1995). Pressure-Temperature paths of the Hidakametamorphic belt (Central and Southern areas) are shown (Osanaï et al., 1992). The numbers within circle correspond to those in Fig. 13.

places orthopyroxene porphyroclasts sequentially from the rim towards the core together with antigorite. Similar evidence of synkinematic talc recrystallization is not observed in ultra fine-grained bands. Talc in these band is formed by the reaction  $En + H_2O = Tlc + Fo$ , and subsequent reaction of  $Tlc + Fo + H_2O = Atg$  is responsible for the present mineral assemblage in ultra fine-grained bands of class 3 deformation microstructure. A schematic model for the formation of syn- and post-kinematic reaction rims around the orthopyroxene porphyroclast is shown in Fig. 13.

It is difficult to determine the thermal condition of class 0-1 shear localization because no synkinematic hydrous reaction can be observed. However, assuming that it was a continuous process prior to the class 1-2 shear localization the deformation condition was probably similar ( $\geq 900^\circ C$ ) or slightly higher temperature. The deformation condition inferred from the lattice preferred orientation of olivine is  $1100^\circ C$ . Although it is not clear whether the class 0-1 shear localization proceeded under dry or wet conditions, many plagioclase segregation veins are found in the Equigranular Zone (Ozawa and Takahashi, 1995, Takahashi, 1997). If these plagioclase segregation vein indicates syn-tectonic melting of peridotites above a wet solidus condition, the class 0-1 shear lo-

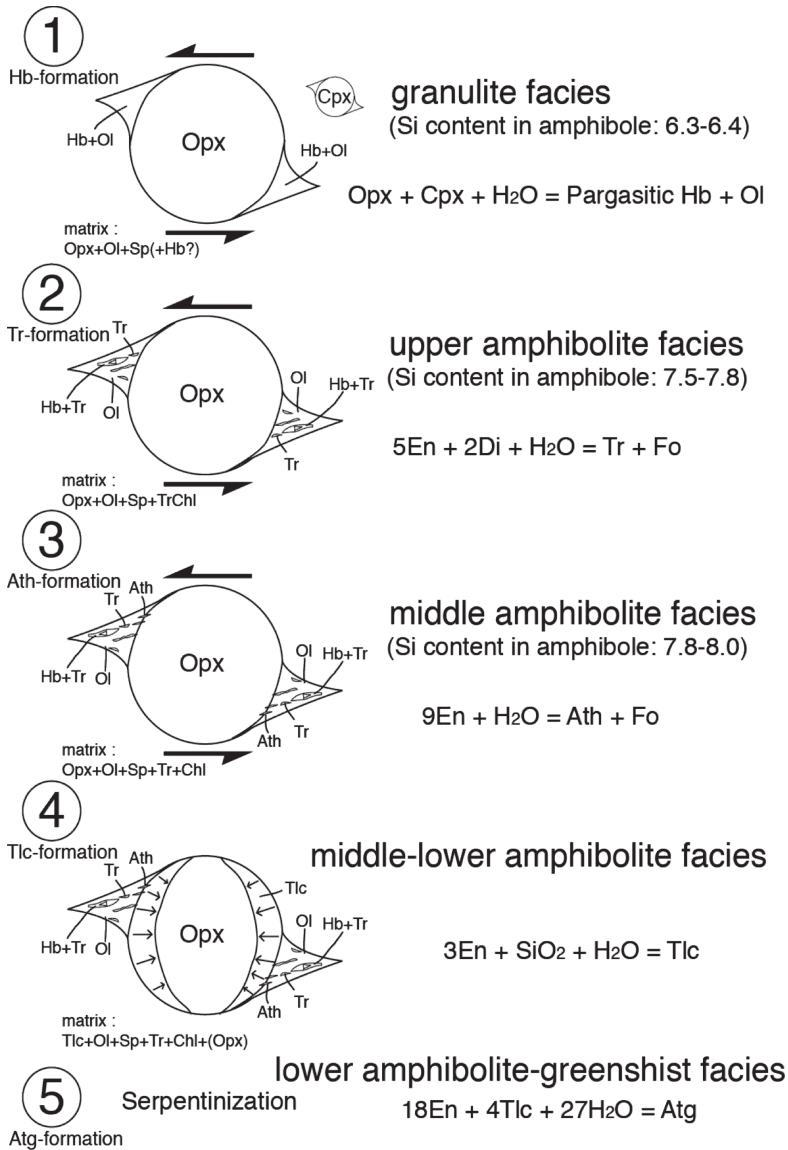


**Fig. 13** Schematic model for the formation of syn- and post-kinematic reaction rims around the orthopyroxene porphyroclast

calization proceeded under wet conditions. Actually a gabbroic part in the plagioclase herzolite in the Upper Zone include extensive pargasite grains (Niida, 1984).

#### 4. 2 Deformation mechanism in shear zones

Deformation mechanism maps are powerful tools for investigating the deformation mechanism and the rheology of rocks (Frost and Ashby, 1982, Karato et al., 1986, Rutter

**Table 2** Flow law parameters for constructing the deformation mechanism maps in Fig. 14, compiled by Drury and Fitz Gerald (1998).

creep	$A$	$n$	$m$	$Q$
<i>Power-law dislocation creep</i>				
Dry [c] slip	$2.884 \cdot 10^4$	3.6	0	535
Dry [a] slip	2.48	3.5	$\geq 0$	385
Wet	$9.55 \cdot 10^3$	3.35	0	444
<i>Diffusion creep</i>				
Dry	$2.46 \cdot 10^{-10}$	1.0	-3	347
Wet	$1.5 \cdot 10^{-12}$	1.0	-3	250

and Brodie, 1988, Handy, 1989). Olivine is most common mineral in the upper mantle. Olivine constitutive flow law and deformation mechanisms have been clarified by experiments under various conditions (dry, wet, wide range of grain sizes, presence of melt etc.). Figure 14 shows deformation mechanism maps constructed for various temperature under conditions for olivine, using the constitutive flow law data of Table 2. The dislocation creep regime is located at higher stress and coarser grain size relative to the diffusion creep regime in each map. The relationship between dynamically recrystallized grain size and stress is shown in each map (Karato et al., 1980).

Since the class 0-1 shear localization is macroscopic textural variation in the complex, it is discussed separately in chapter 10. Here we discuss the deformation mechanism in class 1-2 and 2-3 shear localization.

Class 1-2 shear localization is clearly associated with hydration reactions (pargasite reaction), therefore wet olivine rheology can be applied to class 2 peridotites (Fig. 14). Olivine grain size which dominates the whole rock rheology in class 2 peridotites is inferred to be ca. 50  $\mu\text{m}$  from the continuous anastomosing matrix composed of Ol + Opx ( $\pm$  Cpx) aggregates. The grain size implies stress of ca. 80 MPa, but the recrystallized grain size vs. stress relationship is not applicable in the diffusion creep regime (Karato and Wu, 1993). Even if the paleopiezometric relation is assumed to be achieved in this condition, the inferred strain rate ( $10^{-7}$  /s) is geologically unreasonable. Thus, following Rutter and Brodie (1988) and assuming a strain rate of  $10^{-13}$  /s which is equivalent to that of class 0-1 shear localization (see chapter 10), the inferred stress in the diffusion creep regime is  $10^{-2} \sim 10^{-3}$  MPa. The deformation condition of class 2 peridotites in Fig. 14 is slightly extrapolated toward the faster strain rate condition considering the increase of strain rate in the shear zone. Shear localization of class 1-2 results in weakening of strength by an order of 3~4 due to grain-size sensitivity in the diffusion creep regime.

Class 3 peridotites preserve the evidence of decrease in deformation temperature

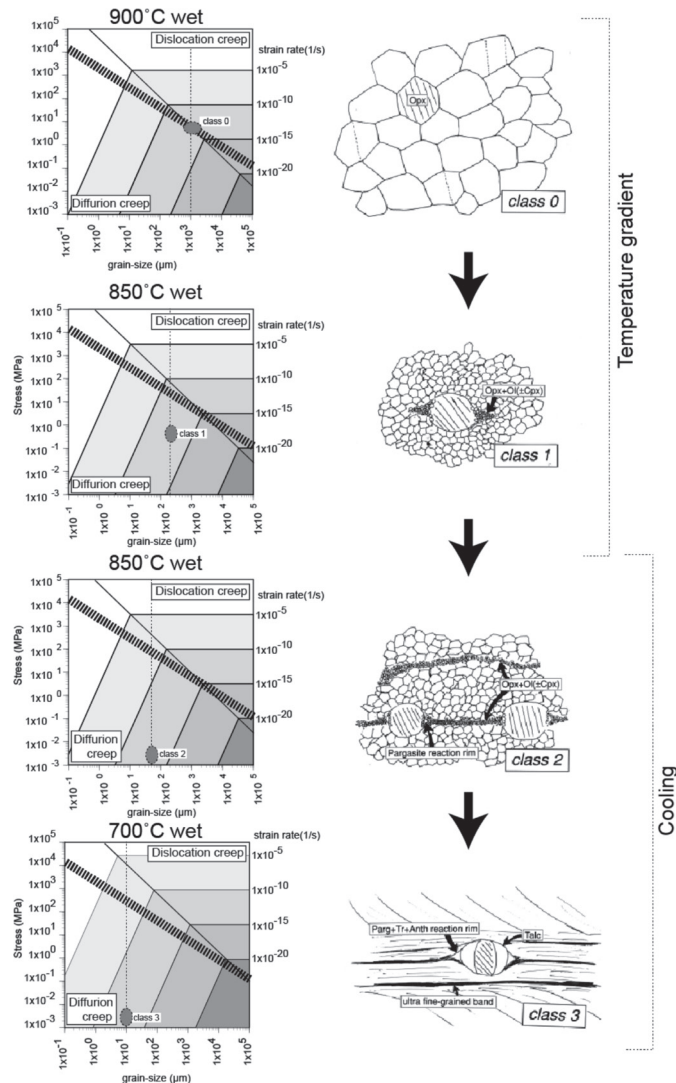


**Fig. 14** Deformation mechanism maps for olivine (700°C, 900°C, 1000°C and 1100°C for wet condition). The deformation conditions for class 0 to 3 are shown by the ellipses on maps.

lasting into the anthophyllite stability condition (ca. 700°C). Olivine grains (ca. 10  $\mu\text{m}$ ) in ultra fine-grained bands are not stable under this condition because grain growth kinetics of olivine in the wet condition is very fast (Karato, 1989). The content of other phases such as Opx and tremolite probably inhibited grain growth of olivine (Handy, 1989, Drury et al., 1991). Temperature and grain size in class 3 also imply stress of  $10^{-2} \sim 10^{-3}$  MPa (Fig. 14). The grain size sensitive diffusion creep dominated by the fine-grained matrix described here is predicted to occur in many shear zones in mantle peridotites, and is thought to be a principal process of strain softening in mantle shear zones

(Handy, 1989, Drury et al., 1991, Vissers et al., 1995, Jaroslow et al., 1996).

### 4.3 Mechanism of shear localization

Shear localization is caused by local increase of strain rate due to either stress-increase or strength-weakening in the shear zone. Possible mechanisms of shear localization involve (i) changes of deformation mechanism due to grain size reduction (dynamic recrystallization, chemical reaction, phase transformation), (ii) heterogeneous change of physical properties (thermal instability, water-weakening by fluid infiltration) and (iii) geometrical change (LPO, reorientation of weak phase in multiphase materials) (Jin et al., 1998). Furthermore, high temperature cataclasis causes high fluid pressure leading to shear localization (Jaroslow et al., 1996). Next, let us consider how each shear localization in the complex has been occurred.

Class 1-2 shear localization is apparently associated with a chemical reaction and fluid infiltration. Recrystallized Opx + Ol ( $\pm$ Cpx) aggregates extending from large Opx grains are not interconnected in class 1. In class 2, however, they form continuous fine-grained bands, and reaction rims of pargasitic hornblende were recrystallized in the vicinity of large Opx grains. Rutter et al. (1985) experimentally produced fibrous amphibole overgrowths on pyroxene grains, but no drastic strain weakening could be observed in this experiment. Shear localization accompanied by strain weakening occurs not only by grain size reduction due to chemical reaction, but also by fine-grained aggregates forming continuous layers which govern whole rock rheology (Drury et al., 1991). Interconnection of fine-grained aggregates requires increase of the fraction of aggregates during deformation. In the case of dynamic recrystallization of olivine, grain-size reduction can potentially occur along all grain boundaries of olivine due to grain boundary bulging or subgrain rotation mechanisms. But in the case of chemical reaction such as for the class 1 or 2 peridotites in this study, grain size reduction can only occur around Opx porphyroclasts. Thus the probability of interconnecting fine-grained aggregates is dependent on the modal abundance of Opx porphyroclasts in peridotites. The modal percent of Opx in class 2 peridotite is higher than that in class 1 (Fig. 4). Therefore class 1-2 shear localization can be explained by the interconnection of recrystallized Opx + Ol ( $\pm$ Cpx) aggregates extending from the Opx porphyroclasts in the peridotites which contain abundant Opx porphyroclasts.

The difference between the matrix in classes 2 and 3 is recognized in grain size and modal abundance of orthopyroxene, tremolite and talc. Because ultra-fine-grained bands in class 3 are thought to be inherited from the fine-grained Opx + Ol ( $\pm$ Cpx) aggregates in class 2, grain size reduction due to the hydration reaction of Opx grains in the aggregates is responsible for the class 2-3 shear localization. Recrystallized tremolite in ultra-fine-grained bands inhibited the grain growth of olivine to maintain the grain size sensitive creep. Dynamic recrystallization of olivine also contributed to the

grain size reduction in class 2-3 shear localization. This process is possibly caused by high temperature cataclastic failure inducing localized high fluid pressure, because class 3 shear zones often crosscut the foliation in class 2 peridotites. Increase of resistance to plastic deformation due to temperature-decrease led to a cataclastic failure.

## 5. CONCLUSIONS

The Horoman peridotite preserves clear relationships between shear localization and metamorphism. I would like to emphasize that the shear localization process was not isothermal, but continued during retrograde conditions of metamorphism over a temperature span of 200°C. Grain-size reduction of olivine in shear zones resulted in weakening of strength by an order of 3-4 due to grain-size sensitivity in the diffusion creep regime. The class 2-3 shear localization persisted down to a temperature of ca. 700°C, i.e. lower than the highest metamorphic condition in granulites surrounding the massif. Therefore, the shear localization into the Internal Shear Zone investigated here must be closely related to the tectonic history of the Hidaka metamorphic belt.

## REFERENCES

- Boillot, G. et al. (1987) Tectonic denudation of the upper mantle along passive margins: a model based on drilling results (ODP leg 103, western Galicia margin, Spain). *Tectonophysics*, 132 : 335-342.
- Brewer, J. A. et al. (1983) BIRPS deep seismic reflection studies of the British Caledonides. *Nature*, 305 : 206-210.
- Drury, M. R. et al. (1991) Shear localisation in upper mantle peridotites. *Pure Applied Geophysics*, 137 : 439-460.
- Drury, M. R. and Fitz Gerald, J. D. (1998) Mantle rheology: Insights from laboratory studies of deformation and phase transition. In *The Earth's Mantle* : 503-559.
- Evans, B. W. (1982) Amphiboles in metamorphosed ultramafic rocks. In *Amphiboles: petrology and experimental phase relations*, eds D. R. Veblen and P. H. Ribbe, Mineral Soc. Am. *Reviews in mineralogy* Vol.9B : 98-113.
- Frost, H. J. and Ashby, M. F. (1982) *Deformation-Mechanism Maps. The Plasticity and Creep of Metals and Ceramics*. Pergamon : 1-184.
- Handy, M. R. (1989) Deformation regimes and the rheological evolution of fault zones in the lithosphere: the effects of pressure, temperature, grainsize and time. *Tectonophysics*, 163 : 119-152.
- Harte, B. (1977) Rock nomenclature with particular relation to deformation and

- recrystallisation textures in olivinebearing xenoliths. *Jour. Geol.*, 85 : 279-288.
- Jaroslów, G. E., Hirth, G. and Dick, H. J. B. (1996) Abyssal peridotite mylonites: implications for grain-size sensitive flow and strain localization in the oceanic lithosphere. *Tectonophysics*, 256 : 17-37.
- Jenkins, D. M. (1981) Experimental phase relations of hydrous peridotites modelled in the system  $\text{H}_2\text{O}-\text{CaO}-\text{MgO}-\text{Al}_2\text{O}_3-\text{SiO}_2$ . *Contributions to Mineralogy and Petrology*, 77 : 166-176.
- Jenkins, D. M. (1983) Stability and composition relations of calcic amphiboles in ultramafic rocks. *Contributions to Mineralogy and Petrology*, 83 : 375-384.
- Jin, D., Karato, S. I. and Obata, M. (1998) Mechanisms of shear localization in the continental lithosphere: inference from the deformation microstructures of peridotites from the Ivrea zone, northwestern Italy. *Journal of Structural Geology*, 20 : 195-209.
- Karato, S. (1989) Grain growth kinetics in olivine aggregates. *Tectonophysics*, 168 : 255-273.
- Karato, S. and Wu, P. (1993) Rheology of the upper mantle: A synthesis. *Science*, 260 : 771-778.
- Karato, S., Paterson, M. S. and Fitz Gerald, J. D. (1986) Rheology of synthetic olivine aggregates: Influence of grain size and water. *Jour. Geophys. Res.*, 71 : 8151-8176.
- Karato, S., Toriumi, M. and Fujii, T. (1980) Dynamic recrystallization of olivine single crystals during high temperature creep. *Geophys. Res. Lett.*, 7 : 649-652.
- Niida, K. (1984) Petrology of the Horoman ultramafic rocks. *Jour. Fac. Sci. Hokkaido Univ. Ser.IV*, 21 : 61-81.
- Osanaï, Y., Owada, M. and Kawasaki, T. (1992) Tertiary deep crustal ultrametamorphism in the Hidaka metamorphic belt, northern Japan. *Journal of Metamorphic Geology*, 10 : 401-414.
- Ozawa, K. and Takahashi, N. (1995) P-T history of a mantle diapir : the Horoman peridotite complex, Hokkaido, northern Japan. *Contributions to Mineralogy and Petrology*, 120 : 223-248.
- Poirier, J. -P. (1980) Shear localization and shear instability in materials in the ductile field. *Journal of Structural Geology*, 2 : 135-142.
- Passchier, C. W. and Trouw, R. A. J. (1996) *Microtectonics*. Springer-Verlag : 1-289.
- Rock, N.M.S. and Leake B.E. (1984) The International Mineralogical Association amphibole nomenclature scheme: computerization and its consequences. *Mineral. Mag.* 48 : 211-227.
- Rubie, D. C. (1983) Reaction-enhanced ductility: the role of solid-solid univariant reactions in deformation of the crust and mantle. *Tectonophysics*, 96 : 331-352.
- Rubie, D. C. (1990) Mechanisms of reaction enhanced deformability in minerals and rocks. *Deformation Processes in Minerals, Ceramics and Rocks* : 262-295.
- Rutter, E. H. and Brodie, K. (1988) The role of tectonic grain size reduction in the

- rheological stratification of the lithosphere. *Geologische Rundschau*, 77 : 295-308.
- Rutter, E. H. and Brodie, K. (1995) Mechanistic interactions between deformation and metamorphism. *Geological Journal*, 30 : 227-240.
- Rutter, E. H. et al. (1985) Experimental 'syntectonic' hydration of basalt. *Journal of Structural Geology*, 7 : 251-266.
- Sawaguchi, T. (2004) Deformation history and exhumation process of the Horoman Peridotite Complex, Hokkaido, Japan. *Tectonophysics*, 379 : 109-126.
- Takahashi, E. and Kushiro, I. (1986) Melting of a dry peridotite at high pressure and basalt magma genesis. *American Mineralogist*, 68 : 859-879.
- Takahashi, N. (1991) Origin of three peridotite suites from Horoman peridotite complex, Hokkaido, Japan; melt segregation and solidification process in the upper mantle. *Journal of Mineralogy, Petrology and Economic Geology*, 86 : 199-215.
- Takahashi, N. (1997) Incipient melting of mantle peridotites observed in the Horoman and Nikanbetsu Peridotite Complexes, Hokkaido, northern Japan. *Jour. Miner. Petrol. Econ. Geol.*, 92 : 1-24.
- Takazawa, E. et al. (1996) Evolution of the Horoman Peridotite (Hokkaido, Japan): Implications from pyroxene compositions. *Chemical Geology*, 134 : 3-26.
- Van der Wal, D. and Vissers, R. L. M. (1993) Uplift and emplacement of upper mantle rocks in the western Mediterranean. *Geology*, 21 : 1119-1122.
- Vissers, R. L. M. et al. (1995) Mantle shear zones and their effect on lithosphere strength during continental breakup. *Tectonophysics*, 249 : 155-171.
- White, S. H., and Knipe, R. J. (1978) Transformation- and reaction-enhanced ductility in rocks. *Journal of Geological Society of London*, 135 : 513-516.
- White, S. H. et al. (1980) On mylonites in ductile shear zones. *Journal of Structural Geology* 2 : 175-187.
- Vissers, R. L. M. et al. (1995) Mantle shear zones and their effect on lithosphere strength during continental breakup. *Tectonophysics*, 249 : 155-171.

## 和文要旨

### かんらん岩に見られる歪集中帯の変形条件・微細構造・レオロジー変化

澤口 隆\*

北海道日高変成帯に露出する幌満かんらん岩体には、kmスケールからcmスケールまでのスケールで階層的に発達する歪集中帯が存在する。これら歪集中帯に発達する変形岩の岩石学的な検討から、歪集中が後退変成作用を伴いながら、グラニュライト相 ( $\geq 900^{\circ}\text{C}$ ) から角閃岩相 (および  $700^{\circ}\text{C}$ ) の条件まで連続したと考えられる。幌満かんらん岩中の歪集中は主要構成鉱物の粒径減少によって3~4桁の歪軟化を引き起こした。